Title: Two-Phase Equation of State for Al2O3

Author(s): Velizhanin, Kirill A.

Intended for: Report

Issued: 2021-08-27

Two-Phase Equation of State for Al_2O_3

Kirill A. Velizhanin*
Theoretical Division, Los Alamos National Laboratory, Los Alamos, NM 87545, USA
(Dated: 08/26/2021)

Two-phase equation of state (EOS) for Al_2O_3 (alumina) is calibrated using the experimental/simulation calibration data uploaded to the *caldata* repository. The two phases are solid α-Al_2O_3 (corundum, sapphire, ruby) and its melt. The enthalpy of formation is set to that available from the NIST-JANAF database at $T = 0\,\mathrm{K}$, $P = 1\,\mathrm{bar}$. The expected applicability range of the EOS is from the ambient conditions to temperatures of $\sim 5000\,\mathrm{K}$ and pressures of $\sim$ 50-100 GPa.

I. GENERAL THEORY

The general description of the EOS models and the calibration procedure is given in detail elsewhere [1], so it is described only very briefly here. The full equation of state (EOS) for the solid α-Al_2O_3(α phase) is described by the Helmholtz free energy

$$A_{solid}(V,T) = A_{cold}(V) + A_{vib}(V,T), \tag{1}$$

where V is the specific (per unit mass) volume and T is the temperature. The "cold" energy, $A_{cold}(V)$, is the energy one would typically obtain from DFT calculations, i.e., it is not just the energy at zero temperature, but it also does not include the zero point energy of lattice vibrations. In Ref. [1], the cold curve was stepwise analytic, i.e., the Birch-Murnaghan form [2] was used in compression, and the so called "Lennard-Jones" form, $A_{cold}(V) = A_0 + \frac{A_1}{V^{a_1}} + \frac{A_2}{V^{a_2}}$, was used in expansion. In this work, the Birch-Murnaghan form is used for the cold energy at all densities, for simplicity. The parameters that need to be specified to fully describe the Birch-Murnaghan cold energy are:

1. V_* - specific volume corresponding to the energy minimum of $A_{cold}(V)$.
2. $E_* = A_{cold}(V_*)$ - the value of energy at the minimum.
3. $K_* = -V\,\frac{dP_{cold}}{dV}\big|_{V=V_*}$ - the "cold" bulk modulus at $V = V_*$, where the "cold" pressure is $P_{cold} = -\frac{dA_{cold}(V)}{V}$.
4. $K'_* = \frac{dK}{dP_{cold}}\Big|_{V=V_*}$ - the pressure derivative of the cold bulk modulus at $V = V_*$.

The Helmholtz free energy corresponding to the lattice vibrations, $A_{vib}(V,T)$, is given by a single Debye model, similar to how the diamond is described in Ref. [1]. The Debye temperature is a function of volume only, thus resulting in the Mie-Grüneisen form of EOS [3]. The dependence of the Debye temperature θ on volume is given by

$$\frac{d\ln\theta}{d\ln V} = -\Gamma(V), \tag{2}$$

where $\Gamma(V)$ is the Grüneisen parameter. The dependence of Γ on V is encoded by two second-order polynomials in V and $1/V$ in compression and expansion, respectively. See Eq. (3) in Ref. [1] and the pertaining discussion. What needs to be specified to fully describe this step-wise polynomial form are:

1. Γ_0 - the value of the Grüneisen parameter at the zero specific volume.
2. Γ_∞ - the value of the Grüneisen parameter at the infinite specific volume.
3. $\Gamma_* = \Gamma(V_*)$ - the value of the Grüneisen parameter at some arbitrary volume where one polynomial is matched with the other. The volume is chosen to be V_* defined above.
4. $\gamma_* = \frac{d\ln\Gamma}{d\ln V}\big|_{V=V_*}$ - the volume derivative of the Grüneisen parameter at $V = V_*$.
5. θ_* - since Eq. (2) is a first order differential equation with respect to θ, one also needs to specify the Debye temperature at the some volume. This volume is again chosen to be V_*, so $\theta_* = \theta(V_*)$ is a parameter to be calibrated.

* kirill@lanl.gov

A. Al_2O_3 melt

Helmholtz free energy for a melt of Al_2O_3 is not introduced independently, but is obtained by modifying that of a solid, Eq. (1). We employ the HighTLiq model which gives the Helmholtz free energy of a melt $A_{melt}(T,V)$ near the melting line by simply shifting the entropy of the solid as [4]

$$A_{melt}(T,V) = A_{solid}(T,V) - \Delta S\left[T - T_m(V)\right]. \tag{3}$$

Other contributions, not shown here, are needed to reproduce the correct asymptotic behavior of heat capacity at $T \gg T_m$ [4]. The dependence of the melting temperature T_m on the specific volume is coming from the Lindemann melting criterion [5]

$$\frac{d\ln T_m}{d\ln V} = 2\left[\frac{1}{3} - \Gamma(V)\right]. \tag{4}$$

Once the solid EOS is specified, the extra EOS parameters needed for its melt are:

1. ΔS - the melting entropy in Eq. (3).
2. $T_{m,*}$ - the melting temperature $T_m(V)$ at some arbitrary reference volume, which is again chosen to be V_*, and so $T_{m,*} = T_m(V_*)$.

Eqs. (1) and (3) are complete single-phase EOS, so any single-phase thermodynamic observable can be obtained directly via thermodynamic differentiation. For example, for pressure one has $P = P(T,V) = -\left(\frac{\partial A}{\partial V}\right)_T$. To compare to single-phase experimental data one often needs to calculate specific volume as a function of pressure, which could be obtained from $P = P(T,V)$ via numerical inversion, effectively yielding $V = V(T,P)$. Finally, such observables as phase boundaries are obtained by evaluating the Gibbs free energy as a function of pressure and temperature, $G_\alpha(T,P) = A_\alpha\left(T, V(T,P)\right) + PV(T,P)$, and then numerically solving $G_\alpha(T,P) = G_\beta(T,P)$, where subscripts $\alpha,\beta = solid,,melt$ denote single-phase EOS. All the above have been implemented within Python-based LANL institutional thermochemical code Magpie [6]. In this work Magpie is used as a Python library that can generate various thermodynamic properties of a multiphase material once models are specified.

II. CALIBRATION

The general calibration procedure is described in detail in Ref. [1]. The calibration data, previously uploaded to the *caldata* repository, maintained by ASC-PEM-HE, is plotted by colored points in Figs. 1 - 4, with the error bars present whenever available. The calibration data from experimental/atomistic simulations is referred to in the figure legends by the first author's last name, the first meaningful word in the title of the publication, and the publication year. For example, Fig. 1 plots the following calibration data for the isobaric thermal expansion: SimmonsSingle1971 [7], GotoElastic1989 [8], AndersonThermoelastic1989 [9] and FiquetHigh1999 [10]. The results corresponding to the calibrated EOS are plotted by black lines in the figures. The left panel in Fig. 2 plots the isothermal compression of the solid Al_2O_3 at constant temperature of $T = 300\,\mathrm{K}$. The calibration data is FingerCrystal1978 [11], JephcoatXray1988 [12], RichetQuasi1988 [13], and DewaeleEquation2013 [14].

The right panel shows the shock Hugoniot for the solid Al_2O_3; the calibration data is MarshLASL1980 [15], ErskineHigh1994 [16], CaoRefractive2014 [17], CaoRefractive2017 [18], and DewaeleEquation2013 [14]. The last set of data is actually not a shock Hugoniot but an isotherm adopted from the left panel and plotted in the right panel to illustrate that a shock Hugoniot of a weakly compressible material almost coincides with the isotherm at not too high pressures.

Constant-pressure heat capacity C_P is plotted in Fig. 3 as a function of temperature at constant pressure $P = 1\,\mathrm{bar}$. The used calibration data is SaxenaAssesed1992 [19]. The solid-liquid melting line is depicted in Fig. 4. The used calibration data is ShenMeasurement1995 [20], AhujaMelting1998 [21], and WangMelting2000 [22].

The calibration data is heterogeneous in a sense that for the same measurement, e.g., the pressure as a function of volume in the shock Hugoniot, Fig. 2(right), some data do not have error bars, some have only pressure error bars, and some have the both pressure and specific volume error bars. Because of this, it is impossible to unambiguously assign calibration weights to the data sets coming from different experiment/simulations. The decision was made to choose a single data set for each type of experiment/simulation that would represent a "typical" result. Only those chosen data sets were used in the calibration procedure. Specifically, FiquetHigh1999 [10], DewaeleEquation2013 [14], MarshLASL1980 [15], SaxenaAssesed1992 [19], and WangMelting2000 [22] datasets were picked out of those plotted in Fig. 1, 2(left, right), 3 and 4, respectively. The last dataset was also limited by the pressure range between

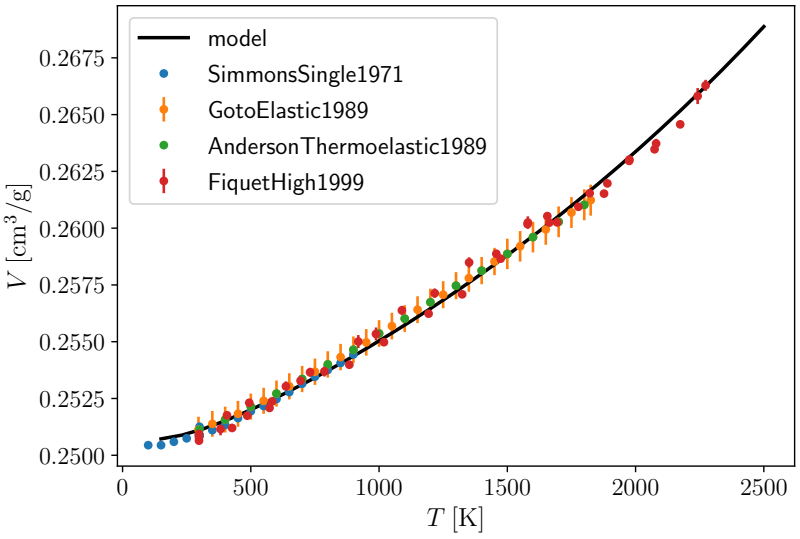

Figure 1. Isobaric thermal expansion at $P = 1\,\text{bar}$.

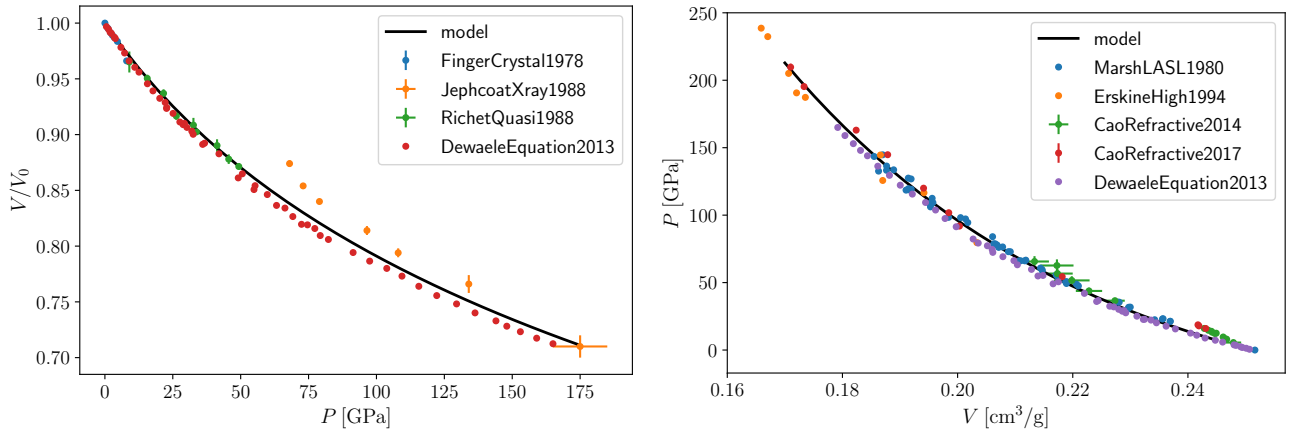

Figure 2. (left) Isothermal compression at $T = 300\,\text{K}$, and (right) shock Hugoniot.

5 GPa and 60 GPa, when performing calibration. The idea behind that was that α-$Al_2O_3$is a complex compound material and so it is unlikely that the HighTLiq model [4] can accurately describe the melting of this material in a wide pressure/temperature range. Therefore, the data range was intentionally limited to that most relevant for the ASC-PEM-HE program (the last "HE" stands for high explosives) to give the HighTLiq model a better chance to fit the melting behavior.

The resulting parameters of the cold curve are given in Tab. I. The calibrated parameters of the lattice contribution

$1/V_*$ [g/cm^3]	E_* [kJ/g]	K_* [GPa]	K'_*
4.0211251494570845	−16.76425920294135	302.35745550830484	3.4796690807468007

Table I. Calibrated parameters of the cold energy.

to the Helmholtz free energy of α-Al_2O_3 are given in Tab. II. The calibrated parameters pertaining to the HighTLiq model are given in Tab. III. Even though the calibration was performed by fitting the model EOS to only selected calibration datasets (one per each experiment type), the model EOS is seen to agree reasonably with all the datasets in Fig. 1, 2(left, right), 3 and 4. The worst agreement is encountered in the solid-liquid phase boundary, Fig. 4, where the calibration data seems to be least reliable (e.g., large error bars). In particular, the model EOS does not seem to accurately reproduce the curvature of the melting line at low pressures. For example, the model produces

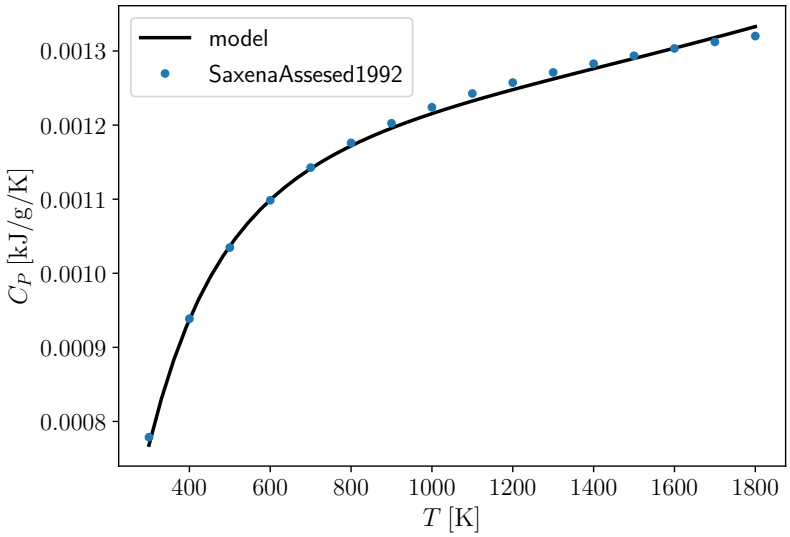

Figure 3. Constant-pressure heat capacity C_P as a function of temperature at $P = 1\,\text{bar}$.

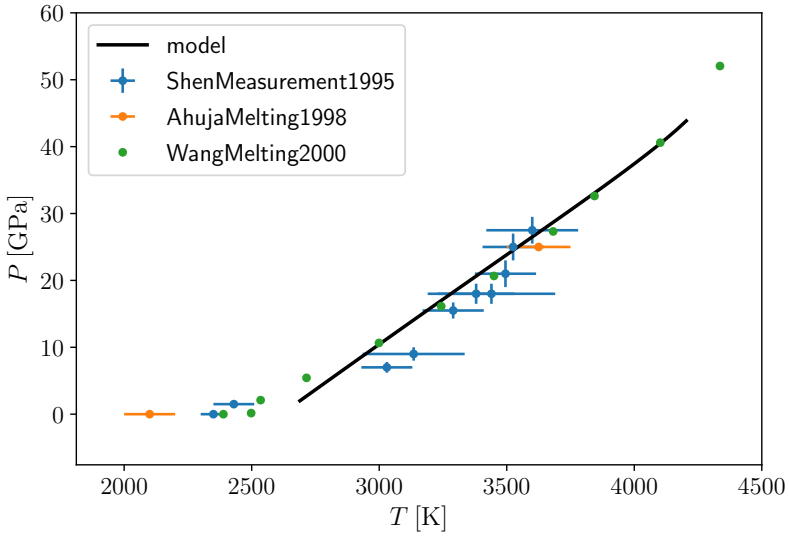

Figure 4. Solid-liquid melting line.

the melting temperature of 2616 K at $P = 1\,\text{bar}$, which is noticeably higher than 2327 K observed experimentally [23]. However, the agreement is better at ASC-PEM-HE-relevant higher pressures.

The absolute energy shift of the Helmholtz free energy, encoded by the E_* parameter of the cold energy model, is irrelevant for all the types of calibration datasets in Figs. 1 - 4. However, the Magpie convention is to calibrate an EOS so that the enthalpy of formation is correct. Magpie assumes that the enthalpy of the standard materials, e.g., Al(fcc), O_2(g), is zero at the Magpie standard state: $T = 0\,\text{K}$, $P = 1\,\text{bar}$. The enthalpy change, $\Delta_f H$, in the following reaction

$$2\text{Al(fcc)} + 1.5\text{O}_2\text{(g)} \rightarrow \alpha\text{-Al}_2\text{O}_3 \tag{5}$$

is then

$$\Delta_f H^\circ = H^\circ\left[\alpha\text{-Al}_2\text{O}_3\right] - 2H^\circ\left[\text{Al(fcc)}\right] - 1.5H^\circ\left[O_2(g)\right] = H^\circ\left[\alpha\text{-Al}_2\text{O}_3\right], \tag{6}$$

where the "$\circ$" superscript denotes the Magpie standard state. The heat of formation for α-Al_2O_3 is $\Delta_f H^\circ =$

Γ_0	Γ_∞	Γ_*	γ_*	θ_* [K]
4/3	1/3	1.2692093277192558	6.076852098526661	982.1351035146715

Table II. The parameter of the Debye model. The values of Γ_0 and Γ_∞ were not obtained from the calibration procedure, their choice is explained in Ref. [1].

$\Delta S/R$	$T_{m,*}$ [K]
7.284526984534509	3897.3797598656547

Table III. The calibrated parameters of the HighTLiq model. The entropy shift of the melt is taken per mole of Al_2O_3 "molecules", and then divided by the gas constant R to yield a dimensionless value.

$-1663.6\,\mathrm{kJ/mol}$ [23], or $-16.316\,\mathrm{kJ/g}$. Accordingly, E_* in Tab. I was chosen so that the solid EOS, Eq. (1), produces the enthalpy of $-16.316\,\mathrm{kJ/g}$ at $T = 0\,\mathrm{K}$, $P = 1\,\mathrm{bar}$.

The entropy of melting, $\Delta S/R \approx 7.28$ in Tab. III is rather large, since the typical "normal melters" have the entropy of melting $\Delta S/R \approx 0.8 \pm 0.1$ [24]. However, the latter entropy is the entropy per mole of *atoms*, and the former one is per mole of Al_2O_3 "molecules". Dividing the obtained melting entropy of Al_2O_3 by 5 (number of atoms in the molecule), we obtain $\Delta S/R/5 \approx 1.46$. This value is still larger than that of normal melters, but is already a reasonable entropy for the so called "anomalous melters" where a change in electronic structure occurs along with melting, e.g., the insulator-to-conductor transition [24]. Very tentatively, as the large scattering of data in Fig. 4 does not allow otherwise, it could be suggested that upon melting Al_2O_3 becomes an atomic (ionic), rather then molecular, conductive liquid with the electronic structure distinct from that of α-Al_2O_3. It can also be noted that the value of entropy of melting obtained here is not too different from the experimental value of $\Delta S/R \approx 5.63$ [25].

ACKNOWLEDGMENTS

Comments from Beth Lindquist and Josh Coe were greatly appreciated. This work was supported by the US Department of Energy through the ASC Program, Los Alamos National Laboratory. Los Alamos National Laboratory is operated by Triad National Security, LLC, for the National Nuclear Security Administration of U.S. Department of Energy (Contract No. 89233218NCA000001).

[1] K. A. Velizhanin and J. D. Coe. Automated fitting of a semi-empirical multiphase equation of state for carbon. *AIP Conf. Proc.*, 2272:070051, 2020.
[2] F. Birch. Finite elastic strain of cubic crystals. *Phys. Rev.*, 71(11):809–824, 1947.
[3] K. A. Velizhanin and J. D. Coe. Equivalent definitions of the mie-gruneisen form. arXiv:2012.01169, 2020.
[4] E.D. Chisolm. A model for liquids in wide-ranging multiphase equation of state. Report, LA-UR-10-08329, Los Alamos National Laboratory, 2010.
[5] O. L. Anderson. *Equations of State of Solids for Geophysics and Ceramic Science*. Oxford University Press, New York, 1995.
[6] C. Ticknor, S. A. Andrews, and J. A. Leiding. Magpie: A new thermochemical code. *AIP Conf. Proc.*, 2272:030033, 2020.
[7] G. Simmons and H. Wang. *Single Crystal Elastic Constants and Calculated Aggregate Properties, Second Edition*, volume 2. The MIT Press, 1971.
[8] T. Goto, O. Anderson, I. Ohno, and S. Yamamoto. Elastic constants of corundun up to 1825 k. *Journal of Geophysical Research*, 94:7588, 1989.
[9] O. L. Anderson, D. L. Isaak, and H. Oda. Thermoelastic parameters for six minerals at high temperature. *Journal of Geophysical Research*, 96:18037, 1989.
[10] G. Fiquet, P. Richet, and G. Montagnac. High-temperature thermal expansion of lime, periclase, corundum and spinel. *Phys Chem Materials*, 27:103, 1999.
[11] L. W. Finger and R. M. Hazen. Crystal structure and compression of ruby to 46 kbar. *Journal of Applied Physics*, 49:5823, 1978.
[12] A. P. Jephcoat, R. J. Hemley, and H. K. Mao. X-ray diffraction of ruby (al2o3:cr 3+) to 175 gpa. *Physica B*, 150:115, 1988.
[13] P. Richet, J. Xu, and H. Mao. Quasi-hydrostatic compression of ruby to 500 kbar. *Physics and Chemistry of Minerals*, 16:207, 1988.
[14] A. Dewaele and M. Torrent. Equation of state of alpha-al2o3. *Physics Review B*, 88:064107, 2013.

[15] S. P. Marsh. Lasl shock hugoniot data. Technical report, 1980.
[16] D. Erskine. High pressure hugoniot of sapphire. *AIP Conference Proceedings*, 309:141, 1994.
[17] X. Cao and et al. Refractive index of r-cut sapphire under shock pressure range 5 to 65 gpa. *J. App. Phys.*, 116:093516, 2014.
[18] X. Cao and et al. Refractive index and phase transformation of sapphire under shock pressures up to 210gpa. *J. App. Phys.*, 121:115903, 2017.
[19] S. K. Saxena and G. Shen. Assessed data on heat capacity, thermal expansion,and compressibility for some oxides and silicates. *Journal of Geophysical Research*, 97:19813, 1992.
[20] G. Shen and P. Lazor. Measurement of melting temperatures of under lower mantle pressures. *Journal of Geophysics Research*, 100:17699, 1995.
[21] R. Ahuja, A. B. Belonoshko, and B. Johansson. Melting and liquid structure of aluminum oxide using a molecular-dynamics simulations. *Phys. Rev. E*, 57:1673, 1998.
[22] Z Wang, H Mao, and S. K. Saxena. The melting of corundum (al2o3) under high pressure conditions. *Journal of Alloys and Compounds*, 299:287 – 291, 2000.
[23] M. W. Chase, Jr., C.A.Davies, J. R. Downey, Jr., D. J. Frurip, R. A. McDonald, and A. N. Syverud. NIST-JANAF thermochemical tables. *J. Phys. Chem. Ref. Data, Monograph 9*, pages 1–1951, 1998.
[24] D. C. Wallace. *Statistical Physics of Crystals and Liquids*. World Scientific, Singapore, 2002.
[25] P.-F/ Paradis, T. Ishikawa, Y. Saita, and S. Yoda. Non-contact thermophysical property measurements of liquid and undercooled alumina. *Jpn. J. Appl. Phys.*, 43(4A):1496–1500, 2004.